Hydrophilic interior between hydrophobic regions in inverse bilayer structures of cation–1,1′-binaphthalene-2,2′-diyl phosphate salts†

Thomas Dorn, Anne-Christine Chamayou and Christoph Janiak*

Received (in Durham, UK) 27th April 2005, Accepted 16th November 2005
First published as an Advance Article on the web 15th December 2005
DOI: 10.1039/b510617f

A series of 1,1′-binaphthalene-2,2′-diyl phosphate ($BNPPA^-$) salts have been synthesized. Their crystal packings show a separation of the hydrophobic naphthyl and hydrophilic $(RO)_2PO_2^-$ phosphate/cation/solvate regions. Hydrogen bonding in the latter is the driving force for "inverse bilayer" formation, with a hydrophilic interior exposing the hydrophobic binaphthyl groups to the exterior. Stacking of the inverse bilayers occurs less through π–π and more through CH···π interactions between the naphthyl groups, which correlates with the formation of thin crystal plates along the stacking direction. Cations used with *R*- or *rac*-$BNPPA^-$ are protonated isonicotin-1-ium amide (**1**), isonicotin-1-ium acid (**2**), guanidinium (**3**), the metal complexes *trans*-tetraammine-dimethanol-copper(II) (**4**), *trans*-diaqua-tetramethanol-copper(II) (**5**) and *cis*-diaqua-bis(ethylene diamine)-nickel(II) (**6**). Crystallization occurs with inclusion of water and methanol solvent molecules, except in **2**. Starting from *R*-BNPPA, inversion takes place with calcium acetate to give **1** as the racemate. **2** is crystallized as the *R*-BNPPA salt. The inversion-symmetrical complex *trans*-$[Cu(H_2O)_2(CH_3OH)_4]^{2+}$ in **5** has Cu–OH_2 bond lengths of 1.937(4) Å, and Cu–O(methanol) of 2.112(4) and 2.167(4) Å, corresponding to a compressed tetragonal geometry.

Introduction

The organization and separation of hydrophobic and hydrophilic regions is a spontaneous process in the formation of monolayers, micelles, bilayers (in membranes) or liposomes from molecules with a polar head and a non-polar tail, *e.g.* phospholipids or detergents (Scheme 1).[1] This organization utilizes many non-covalent interactions, including hydrogen bonding.

The use of supramolecular interactions to mimic such a natural organization process in molecular crystals is a challenge in crystal engineering.[2,3] In this respect, we have synthesized and structurally characterized salts **1–6** of the 1,1′-binaphthalene-2,2′-diyl phosphate (BNPPA) anion, which has a polar phosphate group and a non-polar binaphthalene-diyl moiety (Scheme 2). The phosphate group is an excellent acceptor of classical O/N–H···O hydrogen bonds,[2,4] whereas the naphthyl group can interact through π···π stacking[5,6] and C–H···π bonding.[7] Our work was influenced by a recent report from S. K. Das *et al.* on the bilayer structure of *ortho*-phenylene diammonium perchlorate[2] and by the seminal work of M. D. Ward *et al.* on layered materials of guanidinium alkane and arenesulfonates.[8] The chiral compound 1,1′-binaphthalene-2,2′-diyl phosphoric acid (BNPPAH) in one of its enantiomeric forms has been employed for the optical resolution of chiral amines[9] and amino acids.[10] We are not aware, however, that $BNPPA^-(H)$ has been used as a supramolecular building block, due to its combination of polar and non-polar functionalities.

Here we report the structures of protonated isonicotinium amide and acid cations with the *rac*- or *R*-BNPPA anion. This furthers the continued interest in hydrogen bonding patterns together with π–π stacking of protonated, cationic nitrogen heterocycles.[11] Furthermore, guanidinium and transition

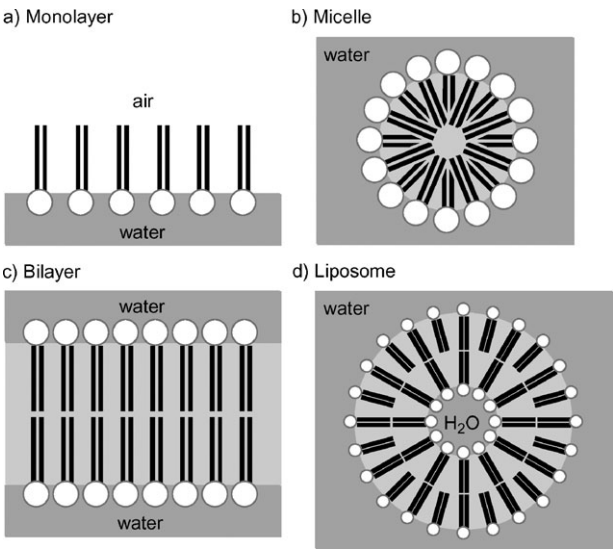

Scheme 1 Molecules with a polar head (○) and a non-polar tail (═) can spontaneously form (a) monolayers, (b) micelles, (c) bilayers and (d) liposome vesicles.

Institut für Anorganische und Analytische Chemie, Universität Freiburg, Albertstraße 21, D-79104 Freiburg, Germany. E-mail: janiak@uni-freiburg.de; Fax: (+49) 761 2036147; Tel: (+49) 761 2036127

† Electronic supplementary information (ESI) available: Annotated pictures of the hydrogen bonding interactions. See DOI: 10.1039/b510617f.

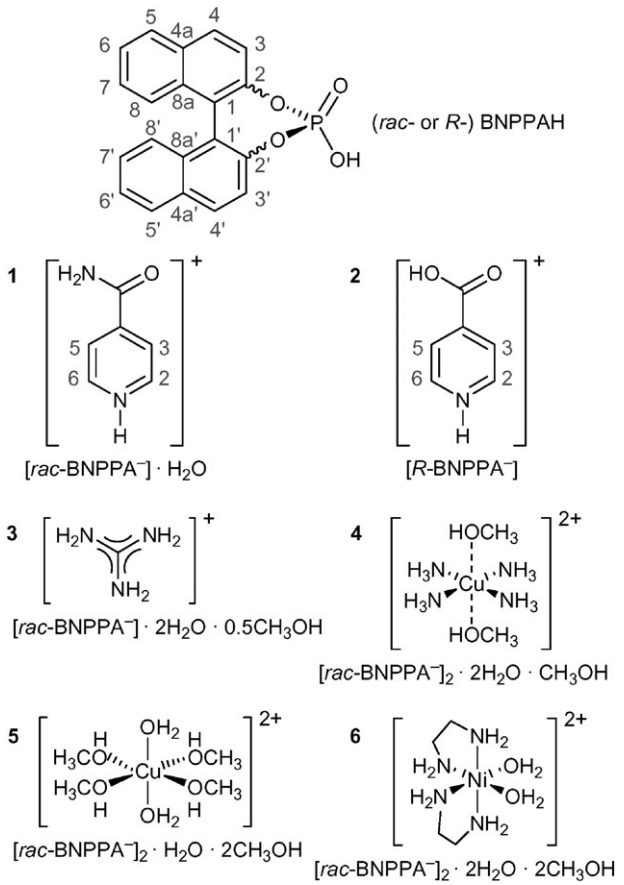

Scheme 2 Molecular composition of the prepared 1,1′-binaphthalene-2,2′-diyl phosphate salts **1–6** with the nomenclature numbering scheme.

metal cations were crystallized with *rac*-BNPPA$^-$ (Scheme 2). The supramolecular inter-cation–anion and inter-anion interactions, such as N/O–H···O, π–π and C–H···π, are analyzed.

Results and discussion

The BNPPA salts **1–6** (Scheme 2) are reproducibly prepared as crystals in good yields within a week through slow solvent evaporation of methanol/water solutions or by a diffusion method.

In the crystallization with isonicotinamide and isonicotinic acid, the *R*-enantiomer of BNPPAH was employed. Crystals of the isonicotinium amide BNPPA$^-$ salt (**1**) did, however, consist of the BNPPA racemate, both according to the X-ray crystallographic refinement and from the absence of a measurable optical rotation. Crystallization of **1** was only successful when calcium acetate was added to the solution and when starting from *R*-BNPPAH. The use of *rac*-BNPPAH yielded an immediate precipitate and no crystals could be obtained. Also, without the addition of calcium acetate, no crystalline product could be obtained from *R*-BNPPAH. The angle of optical rotation of the solution of *R*-BNPPAH/isonicotinamide/calcium acetate was measured during evaporation of the methanol/water mixture until crystallization started. This value was compared to the optical rotation of a *R*-BNPPAH

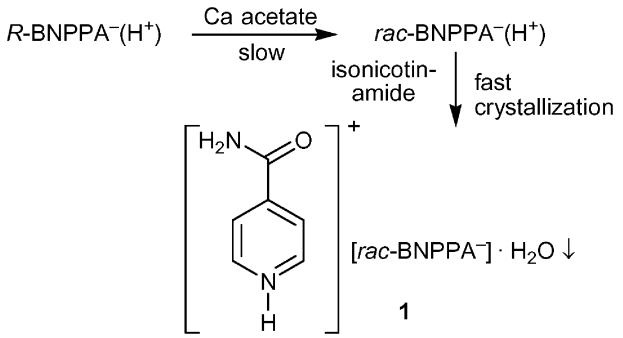

Scheme 3 Suggested relative rates for racemization and crystallization during the formation of **1**.

solution in methanol/water, from which, under otherwise identical conditions, the solvent was evaporated. In both solutions, the optical rotation increased with concentration, and within experimental error, these two values were identical. This excludes the possibility of a fast racemization in solution. Yet when the crystals of **1** were dissolved again, they did not show an optical rotation. From the above observations we conclude that calcium acetate slowly catalyzes the racemization. With both enantiomers available, crystallization proceeds in a quick yet controlled manner through the relatively slow supply of *S*-BNPPA$^-$ (Scheme 3). Further investigations on the process of racemization in *R*-BNPPAH will be carried out.

From isonicotinic acid and *R*-BNPPAH, crystals of **2** could be obtained in the presence of guanidinium chloride without racemization. Many more attempts were made to crystallize *R*-BNPPA$^-$ with the various cations found in **1–6**, but all failed. Compared to the facile crystallization from *rac*-BNPPAH, we encountered difficulties when trying to crystallize from *R*-BNPPAH[12] that were consistent with the difficulties we experienced when trying to crystallize related *R*- or *S*-1,1′-bi-2-naphtholate metal salts.[13] This failure is also contrary to the use of *S*-BNPPAH as a good optical resolution agent for amines and its application in the resolution of pharmaceutical intermediates by fractional crystallization.[9,10]

The phosphate salts **1** and **3–6** form as dihydrates, the latter also as methanol solvates. We trace this finding to the good hydrogen acceptor properties of the polar phosphate group. A Cambridge Structure Database study has recently shown that hydrate formation is above average (~40% and 36%) for pyridinium chloride and phosphate salt structures, respectively, when compared to the total of pyridinium salts (22% hydrate formation).[14] In the following structures, we will compare and interpret the crystal packing based on the supramolecular interactions found.

Crystal packing and hydrogen bonding

Generally, the packing arrangements found in **1–6** can be rationalized by a separation of the hydrophobic binaphthyl backbone of BNPPA from the hydrophilic $(RO)_2PO_2^-$ phosphate groups, cation and solvate components.[2,12]

Figs. 1–6 show projections of the unit cell crystal packings of compounds **1–6**, respectively, to illustrate the lamellar or

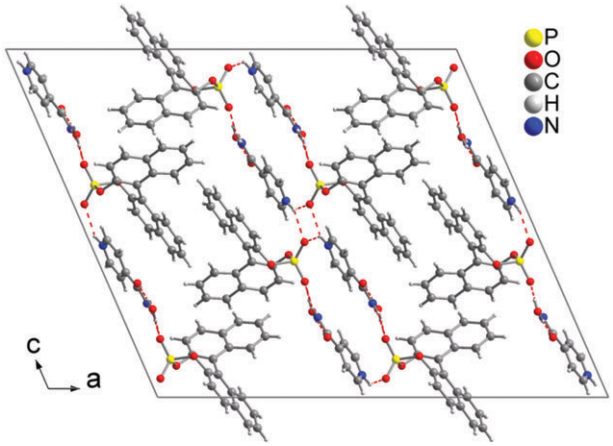

Fig. 1 Projection of the crystal packing in **1** onto the (0 1 0) plane. Hydrogen bonds are indicated with red dashes.

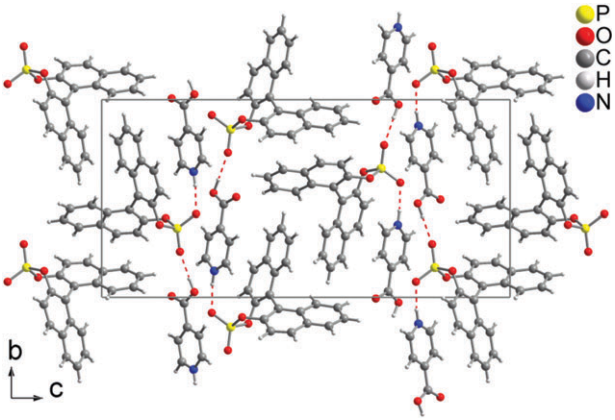

Fig. 2 Projection of the crystal packing in **2** onto the (1 0 0) plane. Hydrogen bonds are indicated with red dashes.

layer-like packing of the hydrophobic and hydrophilic regions. The latter are also highlighted by the hydrogen bonding network shown as red dashes. Details of the hydrogen bonding in **1–6** are listed in Tables 1–4. Annotated pictures of the hydrogen bonding interactions can be found in the supplementary material.† Other bond lengths and angles can also be found in the CIF files, which are also part of the supplementary material.‡ We note that in **1–6**, the P–O(C) bonds average 1.614 Å (with a maximum of 1.627 Å and a minimum of 1.607 Å), while the terminal P–$O^{(-)}$ bonds, with their partial double bond character, average 1.484 Å (with a maximum of 1.494 Å and a minimum of 1.472 Å). Hydrogen bonding to phosphate occurs essentially only to the terminal P–$O^{(-)}$ bonds, with each oxygen atom typically accepting 2–3, and rarely 4, hydrogen bonds.[15] The only exception is the isonicotinium acid structure **2**, where, in the absence of solvent molecules of crystallization,

‡ CCDC reference numbers: 286354 for **1**, 286355 for **2**, 286356 for **3**, 286357 for **4**, 286358 for **5**, 286359 for **6** at 100 K and 286360 for **6** at 203 K. For crystallographic data in CIF or other electronic format see DOI: 10.1039/b510617f

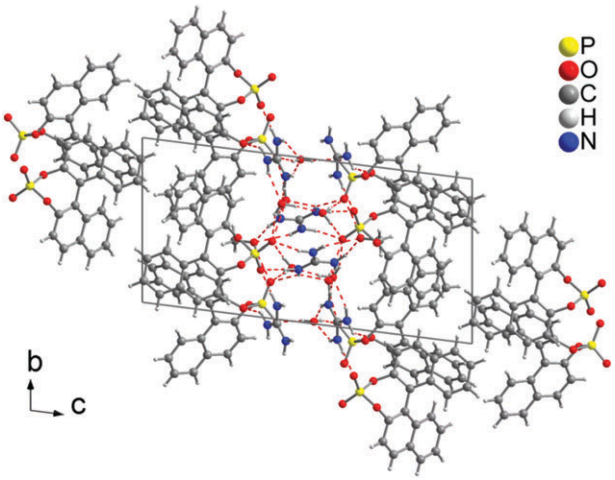

Fig. 3 Projection of the crystal packing in **3** onto the (1 0 0) plane. Hydrogen bonds are indicated with red dashes.

there is only one hydrogen bond to each terminal oxygen atom.

A brief statistical analysis of the unambiguously determined N/O(–H)-donor···O-acceptor distances in **1–6**, shown in Fig. 7, indicates the higher number of hydrogen bonds to phosphate, as well as their shorter donor···acceptor contacts. We trace this to the fact that the hydrogen bond acceptor strength of oxygen follows the sequence $O^- > O$.[12,16] The additional electrostatic attraction leads to shorter H···O^- than H···O contacts.

Compound **5** contains the *trans*-$[Cu(H_2O)_2(CH_3OH)_4]^{2+}$ cation (Fig. 8). For Cu(II), a Jahn–Teller distortion is to be expected, which generally manifests itself in a tetragonal elongated octahedron. The elongated axial bonds are typically longer by 0.3–0.6 Å over the equatorial Cu–ligand bonds.[17] In the complex cation $[Cu(H_2O)_2(CH_3OH)_4]^{2+}$, the three crystallographically different Cu–O bond lengths differ somewhat less with $Cu–O_{H_2O}$ = 1.937(4) Å, and $Cu–O_{CH_3OH}$ = 2.112(4) and 2.167(4) Å. Furthermore, the variation is such that a tetragonal compressed octahedron results, which is a rare example for Cu(II) complexes.[18–22] Together with regular –3-symmetrical Cu(II) structures,[23,24] a tetragonally-distorted

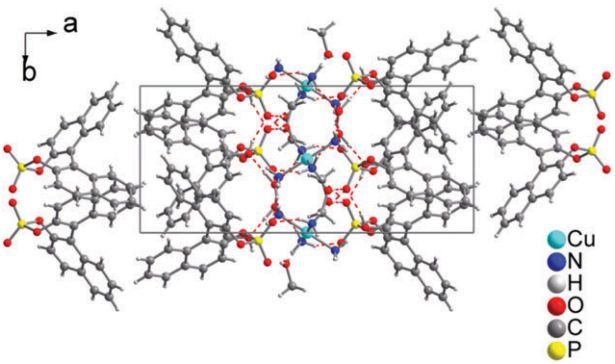

Fig. 4 Projection of the crystal packing in **4** onto the (0 0 1) plane. Hydrogen bonds are indicated with red dashes.

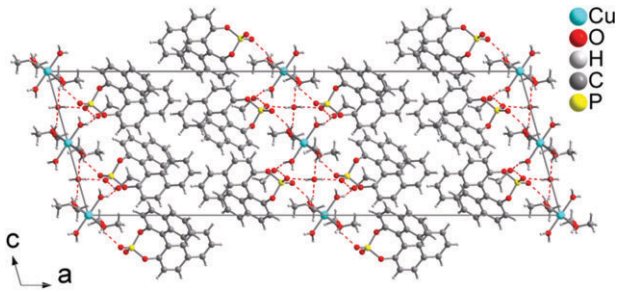

Fig. 5 Projection of the crystal packing in **5** onto the (0 1 0) plane. Hydrogen bonds are indicated with red dashes.

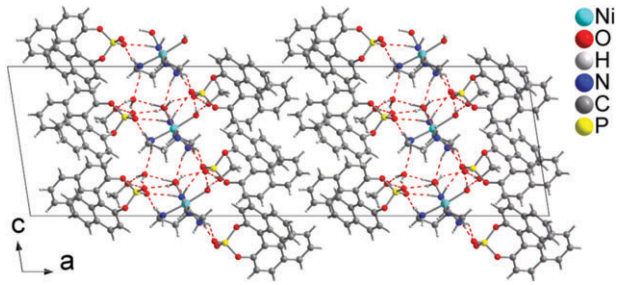

Fig. 6 Projection of the crystal packing in **6** onto the (0 1 0) plane. Hydrogen bonds are indicated with red dashes.

compressed octahedron is usually evidence of a *dynamic* Jahn–Teller distortion.[25,26] Variable temperature single crystal or EPR studies then show an interchange to a second distortion. When the compressed octahedron is observed at room temperature, the elongated octahedron is found at lower temperature.[18,22]

If the atom ligated to a Jahn–Teller active metal center is oscillating between short and long distances, then the anisotropic displacement parameters of the ligated atom along the metal–ligand bond should show considerably more displacement than the Cu atom. An elongated thermal ellipsoid for the ligated atom towards the metal center would indicate either an unresolved static disorder or a dynamic Jahn–Teller disorder.[23–25] For the cation *trans*-$[Cu(H_2O)_2(CH_3OH)_4]^{2+}$ in **5**, a visual inspection of Fig. 8 has to be augmented by a comparison ($\Delta_{A,B}$) of the mean square vibration amplitudes $z^2_{A,B}$ and $z^2_{B,A}$ for the bonded pair of atoms A and B (with $z_{A,B}$ as the radius of the vibration ellipsoid of atom A along the vector from A to B). This is known as the "Hirshfeld Rigid-Bond" test, and with true vibrational ellipsoids should give $\Delta_{A,B} = z^2_{A,B} - z^2_{B,A} \cong 0$, since from the "rigid-bond postulate", the relative vibrational motion of a pair of bonded atoms has an effectively vanishing component in the direction of the bond. Hence, the mean square vibrational amplitudes of a pair of bonded atoms should be equal along the bond direction, but can differ in other directions due to bond bending or torsional vibrations.[27] For the three crystallographically different Cu–O bond lengths in the $[Cu(H_2O)_2(CH_3OH)_4]^{2+}$ component of **5**, $\Delta_{A,B}$ is 24(21) $\times 10^{-4}$ Å^2 for Cu–O_{H_2O}, and is 136(24) and 205(30) $\times 10^{-4}$ Å^2 for the two Cu–O_{CH_3OH} bonds. The large $\Delta_{A,B}$ values for Cu–O_{CH_3OH} indicates either a considerable relative motion (signifying the presence of a dynamic Jahn–Teller effect) or a static disorder between the atoms involved.[25] Further investigations on this matter in compound **5** will be carried out.

The crystal structure of compound **6** is noteworthy because with independent crystallographic data sets collected at 100(2) and 203(2) K, refinement was only successful as a racemic twin in the non-centrosymmetric polar space group *Cc* (see Experimental section—X-Ray crystallography).[28] The unit cell contains both enantiomers *R*- and *S*-$BNPPA^-$, as well as Δ- and Λ-*cis*-$[Ni(en)_2(H_2O)_2]^{2+}$ as independent molecules. Both respective configurations alternate along the c-axis, as shown in Fig. 9. Thus, the structure does *not* present an example of spontaneous resolution from a racemic mixture. The non-centrosymmetric polar packing is due to the identical orientation of the $[Ni(en)_2(H_2O)_2]^{2+}$ cations with their aqua ligands along the polar c-axis (see Fig. 6). This identical alignment can be traced to the hydrogen bonding interactions between adjacent complexes, either direct from an NH_2 group to the aqua ligand or transmitted *via* a phosphate group or a solvate water molecule (Fig. 10).

Table 1 Hydrogen bonding interactions in **1** and **2**[a]

D–H···A	D–H/Å	H···A/Å	D···A/Å	D–H···A/°
1, N/O–H···O(phosphate):				
N1–H1···O4	0.90(3)	2.14(3)	2.917(2)	144(2)
N1–H1···O4^5	0.90(3)	2.39(3)	3.027(3)	128(2)
N2–H2B···O3^6	0.88(3)	2.19(3)	3.058(2)	168(2)
O6–H6A···O3^6	0.88(3)	1.92(3)	2.775(2)	164(3)
1, N/O–H···O(water, amide):				
N2–H2A···O6^1	0.91(3)	2.20(3)	3.105(3)	179(2)
O6–H6B···O5	0.92(3)	1.90(3)	2.815(2)	174(3)
Symmetry transformations: 1 = $x, y-1, z$; 5 = $-x, -y, -z$; 6 = $x, 1-y, z-\frac{1}{2}$				
2, N/O–H···O(phosphate):				
N–H···O3	0.92(6)	1.77(6)	2.640(5)	156(6)
O5–H51···O4^1	0.90	1.84	2.744(6)	173
Symmetry transformation: 1 = $x, y-1, z$				

[a] D = donor, A = acceptor. For found and refined atoms the standard deviations are given.

Table 2 Hydrogen bonding interactions in **3**[a]

D–H···A	D–H/Å	H···A/Å	D···A/Å	D–H···A/°
3, N/O–H···O(phosphate):				
N1–H1B···O4	0.94(2)	2.16(2)	3.072(3)	162(2)
N2–H2A···O3	0.95(2)	1.94(2)	2.871(3)	167(2)
N2–H2B···O7	0.88(2)	2.34(2)	2.965(3)	128(2)
N5–H5B···O3	0.93(3)	1.98(3)	2.899(3)	168(2)
N6–H6A···O5	0.90(3)	2.49(3)	3.081(3)	124(2)
O9–H9B···O4	0.84(3)	2.10(3)	2.889(3)	156(3)
O10–H10A···O8[1]	0.91(3)	1.91(3)	2.811(3)	171(3)
O10–H10B···O4	0.76(3)	2.52(3)	3.165(3)	143(3)
O11–H11A···O4[1′]	0.89(3)	2.03(3)	2.879(3)	158(3)
O11–H11B···O7	0.80(3)	2.19(3)	2.984(3)	168(3)
O12–H12A···O8	0.77(2)	2.17(3)	2.905(2)	160(3)
O12–H12B···O8[2]	0.85(3)	2.04(3)	2.874(3)	167(3)
O13–H13A···O7	0.85(3)	1.86(3)	2.688(3)	164(3)
3, N/O–H···O(water, methanol):				
N1–H1A···O13[2]	0.88(2)	2.41(2)	3.109(3)	136(2)
N2–H2B···O10[2′]	0.88(2)	2.51(3)	3.184(3)	134(2)
N3–H3A···O13[2′]	0.93(2)	1.93(3)	2.814(3)	159(2)
N3–H3B···O10[2′]	0.89(2)	1.91(3)	2.775(3)	161(3)
N4–H4A···O12[2″]	0.88(2)	2.11(3)	2.915(3)	152(2)
N4–H4B···O9[1″]	0.90(2)	2.16(3)	2.947(3)	145(2)
N5–H5A···O12[2″]	0.93(2)	2.21(3)	3.012(3)	143(2)
N6–H6B···O9[1″]	0.93(2)	2.14(3)	2.972(3)	149(3)
O9–H9A···O11[2′]	0.91(3)	1.86(3)	2.768(3)	173(3)
O10–H10B···O9	0.76(3)	2.51(3)	3.171(3)	146(3)

Symmetry transformations: 1 = $x, 1+y, z$; 1′ = $1+x, y, z$; 1″ = $x, -1+y, z$; 2 = $1-x, -y, 1-z$; 2′ = $1-x, 1-y, 1-z$; 2″ = $-x, -y, 1-z$

[a] D = donor, A = acceptor. For found and refined atoms the standard deviations are given.

Table 3 Hydrogen bonding interactions in **4** and **5**[a]

D–H···A	D–H/Å	H···A/Å	D···A/Å	D–H···A/°
4, N/O–H···O(phosphate):				
N1–H1A···O3[2]	0.90	2.30	3.155(6)	158
N1–H1B···O4	0.90	2.28	3.122(5)	155
O5–H5A···O3	0.83	2.00	2.821(5)	171
O6–H6B···O4	0.91	1.83	2.711(6)	162
O7–H7A···O3	0.83	1.88	2.651(6)	155
4, N/O–H···O(water, methanol):				
N1–H1C···O6[2]	0.90	2.31	3.195(7)	168
N2–H2C···O6[3]	0.90	2.30	3.169(7)	164
O6–H6A···O7[1]	0.95(6)	1.76(6)	2.703(7)	172(7)

Symmetry transformations: 1 = $x, 1+y, z$; 2 = $1-x, y+\frac{1}{2}, -z+\frac{3}{2}$; 2′ = $1-x, y-\frac{1}{2}, -z+\frac{3}{2}$; 3 = $1-x, 1-y, 2-z$

5, O–H···O(phosphate):				
O5–H51···O4[1]	0.93(4)	1.74(4)	2.662(5)	170(6)
O6–H61···O4[2]	0.83	1.99	2.721(5)	147
O8–H81···O3	0.86(5)	1.92(5)	2.774(4)	172(6)
O9–H91···O3	0.78(6)	1.93(6)	2.679(5)	162(7)
5, O–H···O(water, methanol):				
O5–H52···O9	0.94(6)	1.76(6)	2.660(6)	161(6)
O7–H71···O8	0.83	1.99	2.748(5)	152

Symmetry transformations: 1 = $x, -1+y, z$; 2 = $-x, -1+y, -z+\frac{1}{2}$

[a] D = donor, A = acceptor. For found and refined atoms the standard deviations are given.

π–π and C–H···π interactions

It is evident that the BNPPA salts **1–6** have a propensity for bilayer packing. The binaphthyl tail-to-tail packing in the hydrophobic lamellar are clearly visible in Figs. 1–6. An earlier example from our work, where $BNPPA^-$ was crystallized with 4,4′-bipyridin-1,1′-ium, showed that this does not necessarily have to be the case.[12] The 4,4′-bipyridin-1,1′-ium dication, with its also polar and non-polar regions, features (hydrophobic) π–π stacking interactions with the naphthyl rings of $BNPPA^-$, which prevents binaphthyl tail-to-tail packing (Fig. 11).

The aromatic naphthyl ring systems in **1–6** lead one to expect the presence of supramolecular π–π and C–H···π interactions.[5–7] The π–π interactions in **1** and **2** are found with short centroid–centroid contacts (Cg···Cg < 3.8 Å), small slip angles ($\beta, \gamma < 25°$) and vertical displacements (d[a] < 1.5 Å), which translate into a sizable overlap of the aromatic plane areas and are indicative of strong π-stacking interactions (Table 5).[5,6] These π-interactions are, however, between naphthyl and isonicotin rings. The only naphthyl π-contacts are found in **3**, albeit between already rather tilted π-planes ($\alpha = 20.1°$). No meaningful naphthyl π-interactions are found in **1**, **2** and **4–6**.

Conversely, C–H···π interactions are found in **1**, **2** and **4–6**. Among C–H···π interactions, the contacts observed here can be classified as "strong", with H···Cg < 2.7 Å and the angle C–H···π-plane > 60° (Table 5).[7] However, the C–H···π interactions remain generally weak "binding" forces, with interaction energies of only 4–10 kJ mol^{-1}.[5,7,29,30]

Hence, we interpret the binaphthyl tail-to-tail packing as being a consequence of the stronger hydrogen bonding interactions between the polar hydrophilic phosphate heads. This hydrogen bonding is clearly seen as the driving force of the bilayer formation and exposes the hydrophobic binaphthyl groups to the exterior (Scheme 5). We call such a bilayer, having a hydrophilic interior and hydrophobic exterior, an "inverse bilayer".[2] The normal phospholipid-type bilayer,

Table 4 Hydrogen bonding interactions in **6** at 100 K[a]

D–H···A	D–H/Å	H···A/Å	D···A/Å	D–H···A/°
6, N/O–H···O(phosphate):				
O1–H1D···O6	0.72	2.11	2.815(4)	164
N1–H1F···O9[4]	0.92	2.34	3.134(4)	145
N2–H2F···O6[2]	0.92	2.38	3.177(4)	145
N3–H3C···O6	0.92	2.15	3.038(4)	163
N3–H3D···O9[4]	0.92	1.98	2.883(4)	167
N4–H4D···O6[2]	0.92	2.33	2.993(4)	128
O11–H11B···O5[1]	0.84	2.04	2.780(4)	147
O11–H11A···O10[4′]	0.78	2.08	2.828(4)	162
O12–H12B···O9[1]	0.88	1.86	2.690(4)	156
O13–H13A···O5[1]	0.84	1.82	2.655(4)	173
O14–H14A···O10	0.84	1.86	2.688(4)	168
6, N/O–H···O(water, methanol):				
O1–H1C···O13	0.74	1.93	2.653(4)	162
O1–H2C···O11	0.79	1.96	2.733(4)	164
O2–H2D···O12[4′]	1.01	1.64	2.655(4)	179
N1–H1E···O12[3]	0.92	2.11	2.985(5)	158
N2–H2E···O11	0.92	2.28	3.116(4)	151
N4–H4C···O2[2]	0.92	2.18	3.049(4)	158
O12–H12A···O14	1.00	1.66	2.648(4)	168

Symmetry transformations: 1 = $x, 1+y, z$; 2 = $x, 1-y, z-\frac{1}{2}$; 3 = $x-\frac{1}{2}, y-\frac{1}{2}, z-1$; 4 = $x-\frac{1}{2}, -y+\frac{1}{2}, z-\frac{1}{2}$; 4′ = $x-\frac{1}{2}, -y+\frac{3}{2}, z-\frac{1}{2}$

[a] D = donor, A = acceptor. For found and refined atoms the standard deviations are given.

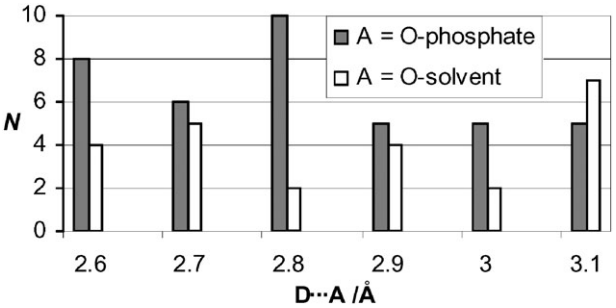

Fig. 7 Number (*N*) of N/O(–H)-donor···O-acceptor (D···A) distances in **1–6** in respective distance intervals. Data plotted from Tables 1–4.

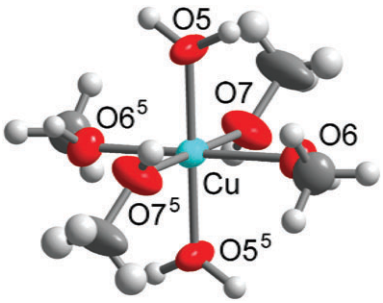

Fig. 8 Coordination polyhedron of $[Cu(H_2O)_2(CH_3OH)_4]^{2+}$ in **5**. Selected bond lengths (Å) and angles (°): Cu–O5 1.937(4), Cu–O6 2.112(4), Cu–O7 2.167(4); O5–Cu–O6 91.97(16), O5–Cu–O6^5 88.03(16), O5–Cu–O7 86.97(17), O5–Cu–O7^5 93.03(17), O6–Cu–O7 87.58(15), O6–Cu–O7^5 92.42(15). Vibrational ellipsoids are drawn at the 50% level; symmetry transformation 5 = $-x$, $-y$, $-z$.

which is depicted in Scheme 1, has a hydrophobic interior and hydrophilic exterior. The weak C–H···π interactions between the hydrophobic exterior regions of adjacent inverse bilayers

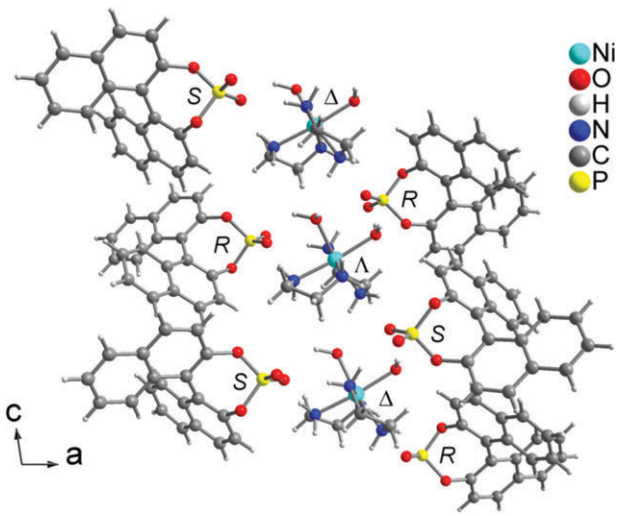

Fig. 9 Section of the crystal packing in **6** showing the alternation of *R*- and *S*-BNPPA$^-$, as well as of Δ- and Λ-*cis*-$[Ni(en)_2(H_2O)_2]^{2+}$ configurations along the c-axis. Hydrogen bonds are not shown for clarity.

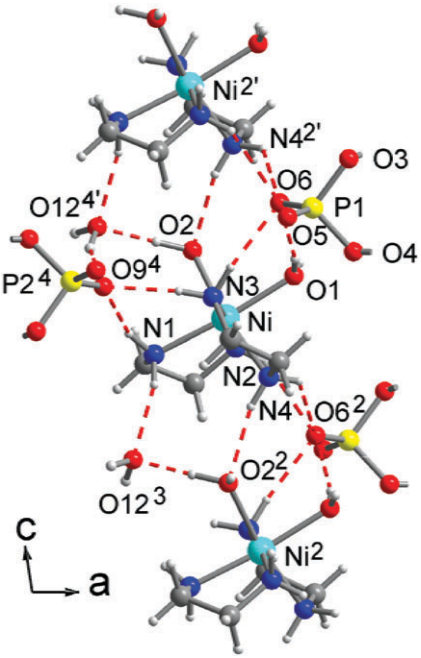

Fig. 10 Hydrogen bonding interactions (*cf.* Table 4) between the $[Ni(en)_2(H_2O)_2]^{2+}$ cations in **6** as the origin of the identical orientation along the c-axis. Additional symmetry transformation: 2′ = x, 1 − y, $z + \frac{1}{2}$

then lead to the crystallization of thin plates of compounds **3–6**. Generally, the thin plate crystal dimension corresponds to the longest crystallographic axis; that is the c-axis for compound **3**, and the a-axis for compounds **4–6** (*cf.* Table 5 and Table 6). This longest crystallographic axis, taken as the horizontal axis in Figs. 3–6, can be seen as the stacking direction for the inverse bilayers in these structures (Scheme 5). In compounds **1** and **2**, isometric crystals result with the somewhat stronger π–π interactions.

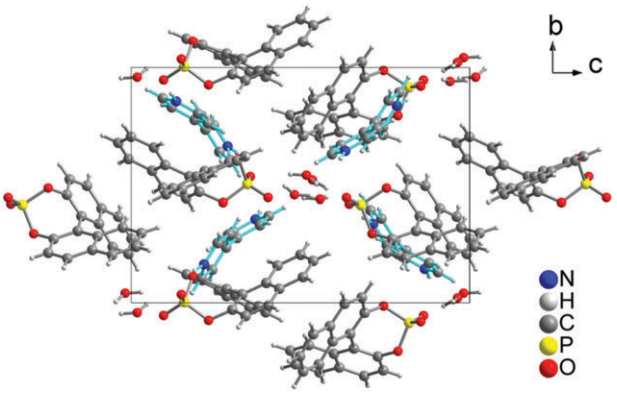

Fig. 11 Projection of the crystal packing in 4,4′-bipyridin-1,1′-ium bis(BNPPA)·2.5H_2O onto the (1 0 0) plane. The pyridyl carbon skeleton is highlighted in light blue. Hydrogen bonds are not shown for clarity.[12]

Table 5 Distances and angles for the strongest π-contacts in the crystal structures of **1–6**[a]

Compound	π–π interactions ring(I)···ring(J)	d[Cg(I)···Cg(J)]/Å[b]	α/°[c]	β/°[d]	γ/°[e]	d[Cg(I)···P(J)]/Å[f]	d[Cg(J)···P(I)]/Å[g]	d[a]/Å[h]
1	Inner-naph2···isonicotin	3.5912	7.76	17.51	25.16	3.250	3.425	1.53, 1.08
	Outer-naph2···isonicotin	3.7657	5.42	24.44	22.39	3.482	3.428	1.43, 1.56
2	Inner-naph2···isonicotin	3.679	9.33	19.69	28.59	3.231	3.464	1.76, 1.24
	Outer-naph2···isonicotin	3.808	4.96	24.20	26.87	3.397	3.474	1.72, 1.56
3	Inner-naph1···outer-naph3[1]	3.819	20.1	14.6	11.3	3.745	3.695	0.75, 0.97
	Symmetry transformation 1 = x, 1 + y, z							
4	No meaningful π–π interactions found (shortest d[Cg(I)···Cg(J)] is 4.93 Å, α > 62°)							
5	No meaningful π–π interactions found (shortest d[Cg(I)···Cg(J)] is 4.78 Å, α > 59°)							
6	No meaningful π–π interactions found (shortest d[Cg(I)···Cg(J)] is 4.92 Å, α > 61°)							

Compound	C–H···π interactions ligand-C–H···ring	d[H···Cg]/Å[i]	d[H···⊥]/Å[j]	γ/°[e]	∠ [CH···Cg]/°[k]	d[C···Cg]/Å[l]	∠[CH···P]/°[m]
1	Outer-naph1-C–H···outer-naph1[6]	2.58	2.52	12.5	171	3.51	76
	Symmetry transformation: 6 = $\frac{1}{2} - x, \frac{1}{2} + y, \frac{1}{2} - z$						
2	Inner-naph1-C–H···outer-naph1[3]	2.58	2.53	11.6	134	3.30	56
	Outer-naph2-C–H···outer-naph1[3′]	2.73	2.68	11.9	141	3.51	60
	Outer-naph2-C–H···outer-naph2[3″]	2.96	2.93	8.5	135	3.68	47
	Symmetry transformations: 3 = $\frac{1}{2} + x, \frac{1}{2} - y, 2 - z$; 3′ = $-\frac{1}{2} + x, -\frac{1}{2} - y, 2 - z$; 3″ = $\frac{1}{2} + x, -\frac{1}{2} - y, 2 - z$						
3	No C–H···ring interactions seen within set limits (H···Cg < 3.0 Å, γ < 30.0°)						
4	Outer-naph1-C–H···inner-naph2[4]	2.60	2.58	6.7	156	3.48	68
	Outer-naph2-C–H···outer-naph1[3]	2.98	2.88	14.8	146	3.79	51
	Symmetry transformations: 3 = $-x, 1 - y, 1 - z$; 4 = $x, \frac{3}{2} - y, -\frac{1}{2} + z$						
5	Outer-naph1-C–H···outer-naph2[7]	2.87	2.85	7.5	144	3.67	51
	Outer-naph2-C–H···inner-naph1[4]	2.82	2.73	14.7	164	3.73	67
	Symmetry transformations: 4 = $x, 2 - y, \frac{1}{2} + z$; 7 = $\frac{1}{2} - x, \frac{3}{2} - y, 1 - z$						
6	Outer-naph1-C–H···inner-naph2[2]	2.70	2.67	8.8	164	3.63	72
	Outer-naph2-C–H···outer-naph4	2.93	2.86	12.5	140	3.71	51
	Outer-naph3-C–H···outer-naph1	2.94	2.88	12.1	141	3.73	52
	Outer-naph4-C–H···inner-naph3	2.65	2.64	4.8	163	3.57	71
	Symmetry transformations: 2 = $x, 1 - y, \frac{1}{2} + z$; 2′ = $x, -y, -\frac{1}{2} - z$						

[a] See Scheme 4 for a graphical depiction of the distances and angles in the assessment of the π-contacts. Aromatic rings of the naphthyl groups are differentiated inner (bonded to PO_4) and outer; the two different naphthyl groups of BNPPA are differentiated as naph1 and naph2, respectively; naph3 and naph4 if two crystallographically different BNPPA anions are present. [b] Centroid–centroid distance. [c] Dihedral angle between the ring planes. [d] Angle between the centroid vector Cg(I)···Cg(J) and the normal to the plane I. [e] Angle between the centroid vector Cg(I)···Cg(J) and the normal to the plane J. [f] Perpendicular distance of Cg(I) on ring plane J. [g] Perpendicular distance of Cg(J) on ring plane I. [h] Vertical displacement between ring centroids; two values if the two rings are not exactly parallel (*i.e.* α ≠ 0°) because of the two reference planes P(J,I). [i] H–centroid distance. [j] Perpendicular distance of H on ring plane. [k] C–H-centroid angle. [l] C–centroid distance. [m] Angle C–H with π-plane P.

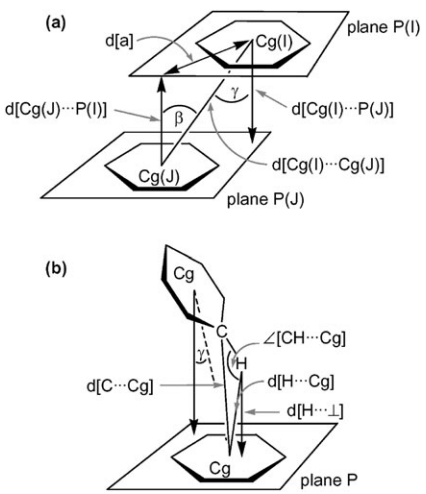

Scheme 4 Graphical presentation of the parameters used in Table 5 for the description of (a) π–π stacking and (b) C–H···π interactions.

Conclusions

The principal interactions controlling the structures of 1,1′-binaphthalene-2,2′-diyl phosphate ($BNPPA^-$) salts with protonated amine or transition metal cations is hydrogen bonding from the cation and solvent molecules to the hydrophilic $(RO)_2PO_2^-$ phosphate head. This hydrogen bonding creates an interior hydrophilic phosphate/cation/solvate region in what is termed an "inverse bilayer", exposing the hydrophobic binaphthyl groups on both exterior sides. The stacking of the inverse bilayers occurs mostly through C–H···π interactions between the naphthyl groups. Because of the general weakness of this type of interaction, crystal growth along this direction does not proceed well. Thus, thin crystal plates form, with the short crystal dimension being the stacking direction of the inverse bilayers. Attempts will be made to replace the weak C–H···π by stronger π-stacking interactions through the addition of appropriate aromatic groups, which should function as a "glue" between the hydrophobic naphthyl regions. In the structure of **5**, hydrogen bonding in the hydrophilic

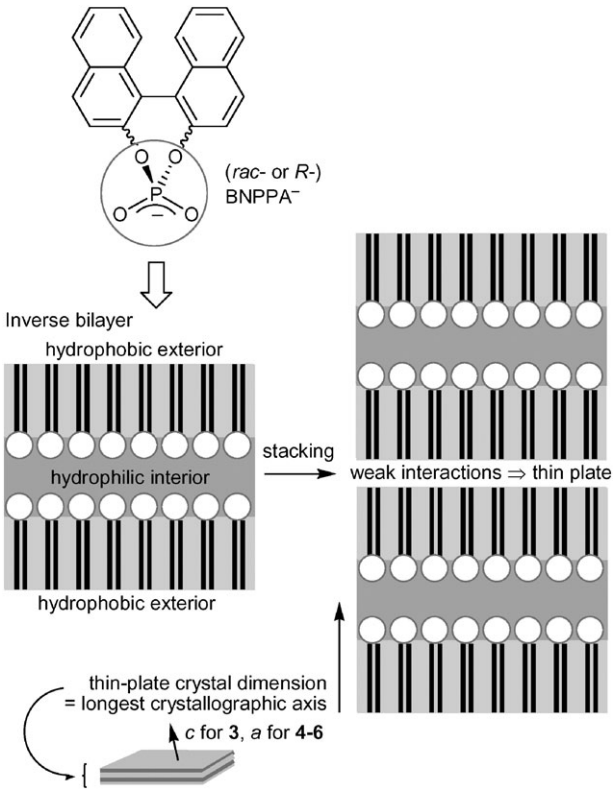

Scheme 5 Inverse bilayer formation and stacking with weak "hydrophobic" interactions to produce a thin crystal plate.

interior stabilizes a compressed tetragonal distortion of the complex *trans*-$[Cu(H_2O)_2(CH_3OH)_4]^{2+}$. The origin of this rare Jahn–Teller distortion will be the subject of further investigations. **6** crystallizes in the polar space group *Cc* due to the identical orientation of the *cis*-$[Ni(en)_2(H_2O)_2]^{2+}$ cations with their aqua ligands along the polar c-axis.

Experimental

Elemental analyses were obtained on a VarioEL from Elementar Analysensysteme GmbH. Elemental analyses were carried out on samples freed from the attached mother liquor but without drying in a vacuum. The samples were measured within hours of being taken from the mother liquor. IR spectra (2–4 mg compound/300 mg KBr pellet) were measured on a Bruker Optik IFS25 from 4000 to 400 cm^{-1}. IR absorptivities are given as w (weak), m (medium) or s (strong). ^1H and ^{13}C NMR spectra were collected on a Bruker Avance DRX 400 (400 MHz for ^1H and 100.6 MHz for ^{13}C with ^1H broad band de-coupling) with calibration against the residual protonated solvent signal (d_6-DMSO: ^1H NMR 2.52 ppm, ^{13}C NMR 39.5 ppm). ^1H NMR multiplicities are stated as s (singlet), d (doublet), t (triplet) or m (multiplet). ^{31}P NMR spectra were obtained on a Bruker Avance DPX 200 at 81 MHz with ^1H broad band de-coupling against an external standard of 85% H_3PO_4. Melting points were measured (up to 180 °C) in open glass capillaries in a melting point apparatus according to Dr. Tottoli, and are uncorrected. The specific angles of optical rotation were obtained on a Perkin-Elmer 241 polarimeter at 25 °C in 0.2 cm quartz cuvettes at the Na-D wave length of 589 nm.

rac-1,1′-Bi-2-naphthol was prepared by the oxidative coupling of 2-naphthol using $FeCl_3 \cdot 6H_2O$ in H_2O at 50 °C and recrystallized from toluene. The analytical data matched literature values.[31] The chemicals guanidinium carbonate (Aldrich), guanidinium chloride (Aldrich), isonicotinamide (EGA-Chemie, Steinheim), isonicotinic acid (Fluka) and *R*-1,1′-bi-2-naphthol (Reuter Chemische Apparatebau KG, Freiburg), along with the solvents and other common reagents, were of reagent grade or better and used without further purification. Ethylene diamine was a technical product and distilled over a 20 cm Vigreux column. Bis(ethylene diamine)nickel nitrate was prepared from $Ni(NO_3)_2 \cdot 6H_2O$ (1.0 g, 3.4 mmol) and ethylene diamine (1.24 g, 20.6 mmol) in 15 cm^3 of water by stirring for 1 h at room temperature, followed by solvent removal and drying in a vacuum.

Syntheses

***rac*- or *R*-1,1′-Binaphthalene-2,2′-diyl phosphoric acid (*rac*- or *R*-BNPPAH).** The compound was synthesized by a modified literature procedure.[32,33] A 250 cm^3 Schlenk flask was evacuated, refilled with argon and charged under argon with a solution of *rac*- or *R*-1,1′-bi-2-naphthol (10 g, 35 mmol in 50 cm^3 of CH_2Cl_2 and 30 cm^3 of pyridine). The solution was cooled to 0 °C in an ice bath and $POCl_3$ (4 cm^3, 6.6 g, 43 mmol) added dropwise. The mixture was heated to reflux for 3 h, then the solvent completely removed (to avoid pyridine and $POCl_3$ residues) in a vacuum. The residue was dissolved in a hot sodium carbonate solution prepared from Na_2CO_3 (15 g) in H_2O (400 cm^3). Finely divided activated carbon (5 g) was added to the solution, the mixture heated to reflux for 20 min in an open flask (to remove any residual pyridine) and filtered hot through a paper filter. After cooling to 5 °C, the solution was acidified dropwise with 12 M hydrochloric acid to yield a colorless precipitate. (Without pre-cooling, a yellow, rather impure oil instead of a colorless powder was obtained.) After stirring for 12 h at room temperature, the precipitate was separated by filtration and dried in a vacuum to yield 10.3 g (85%) of a finely powdered colorless solid (m.p. > 180 °C). $C_{20}H_{13}O_4P$ (348.3): calc. C, 68.97; H, 3.76; found C, 67.79; H, 3.89%. ^{31}P NMR (d_6-DMSO): 4.5. $[\alpha]^{25} = -594°$ cm^2 g^{-1} (measured at 2.3 mg cm^{-3} in CH_3OH). Literature values: $[\alpha] = -530$,[34] −601 and −609° (all in CH_3OH).[33]

(Isonicotin-1-ium amide)-(*rac*-1,1′-binaphthalene-2,2′-diyl phosphate)·monohydrate, $(C_6H_7N_2O)(C_{20}H_{12}PO_4) \cdot H_2O$ (1). *R*(!)-BNPPAH (0.069 g, 0.20 mmol), calcium acetate (0.0158 g, 0.10 mmol) and isonicotinamide (0.0244 g, 0.2 mmol) were dissolved in a mixture of 10 cm^3 methanol and 10 cm^3 H_2O. Solvent evaporation from an open vial at room temperature yielded colorless to very light-yellow crystals after a few days (yield 0.05 g, 51%, average from four batches) (m.p. > 180 °C). The use of *rac*-BNPPAH yielded an immediate precipitate and no crystals could be obtained. Also, without the addition of calcium acetate, no crystalline product could be obtained. $C_{26}H_{21}N_2O_6P$ (488.42): calc. C, 63.94; H, 4.33; N, 5.74; found C, 62.64; H, 4.62; N, 6.49%. IR (cm^{-1}): 1684 (s), 1627 (m), 1591 (s), 1507 (m), 1464 (m), 1388 (m), 1331 (m), 1242 (s), 1086 (m), 960 (m), 842 (m) and 816 (m). ^1H NMR (d_6-DMSO): 8.79 (s, 2 H, isonicotinium-H2/6), 8.30 (s, 1

Table 6 Crystal data and structure refinement for compounds **1–5**

Compound	**1**	**2**	**3**	**4**	**5**
Empirical formula	$C_{26}H_{21}N_2O_6P$	$C_{26}H_{18}NO_6P$	$C_{43}H_{48}N_6O_{13}P_2$[e]	$C_{43.5}H_{54.5}CuN_4O_{14}P_2$	$C_{46}H_{54}CuO_{17}P_2$
M/g mol^{-1}	488.42	471.38	918.81	982.89	1004.37
Crystal size/mm	0.46 × 0.16 × 0.08	0.45 × 0.21 × 0.12	0.40 × 0.19 × 0.09	0.36 × 0.19 × 0.03	0.57 × 0.18 × 0.03
θ range/°	1.55–27.30	1.60–26.40	0.98–28.81	1.97–25.10	1.01–26.05
h; k; l range	−36, 36; −8, 8; −31, 31	−8, 8; −15, 15; −31, 30	−13, 13; −15, 14; −28, 28	−24, 24; −10, 10; −14, 14	−51, 51; −10, 10; −16, 16
Crystal system	Monoclinic	Orthorhombic	Triclinic	Monoclinic	Monoclinic
Space group	$C2/c$	$P2_12_12_1$	P-1	$P2_1/c$	$C2/c$
a/Å	28.659(5)	6.8200(11)	10.0813(15)	20.867(2)	41.876(6)
b/Å	6.8903(12)	12.3523(19)	11.2429(17)	9.1006(11)	8.6579(13)
c/Å	24.209(4)	25.480(4)	21.107(3)	12.2266(14)	13.225(2)
α/°	90	90	93.363(3)	90	90
β/°	113.548(3)	90	98.274(3)	97.654(2)	105.860(3)
γ/°	90	90	112.770(3)	90	90
V/Å^3	4382.5(13)	2146.5(6)	2165.7(6)	2301.2(5)	4612.5(12)
Z	8	4	2	2	2
D_{calc}/g cm^{-3}	1.481	1.459	1.409	1.419	1.446
F(000)	2032	976	964	1029	2100
μ/mm^{-1}	0.175	0.174	0.174	0.614	0.617
Maximum/minimum transmission	0.9862/0.9243	0.9792/0.9262	0.9850/0.9330	0.9842/0.8101	0.9805/0.7180
Reflections collected	18427	17700	19709	16523	17890
Independent reflections	4913 (R_{int} = 0.0476)	4414 (R_{int} = 0.0479)	10115 (R_{int} = 0.0519)	4094 (R_{int} = 0.0877)	4565 (R_{int} = 0.0793)
Observed reflections [$I > 2\sigma(I)$]	3247	2736	4815	2342	2483
Parameters refined	331	310	640	301	294
Maximum/minimum $\Delta\rho$[a]/e Å^{-3}	0.240/–0.367	0.494/–0.756	0.361/–0.437	0.968/–0.575	0.533/–0.635
R_1/wR_2 [$I > 2\sigma(I)$][b]	0.0408/0.0900	0.0638/0.1093	0.0490/0.0553	0.0599/0.1107	0.0591/0.1005
R_1/wR_2 (all reflections)[b]	0.0780/0.1051	0.1214/0.1299	0.1333/0.0659	0.1384/0.1332	0.1475/0.1295
Goodness-of-fit on F^2[c]	0.997	1.103	1.113	1.162	1.283
Weighting scheme w; a/b[d]	0.0450/2.9810	0.0000/3.4270	0.0000/0.0000	0.0000/7.7841	0.0000/21.2945

[a] Largest difference peak and hole. [b] $R_1 = [\Sigma(\|F_0\| - \|F_c\|)/\Sigma|F_0|]$; $wR_2 = [\Sigma[w(F_0^2 - F_c^2)^2]/\Sigma[w(F_0^2)^2]]^{\frac{1}{2}}$. [c] Goodness-of-fit = $[\Sigma[w(F_0^2 - F_c^2)^2]/(n-p)]^{\frac{1}{2}}$. [d] $w = 1/[\sigma^2(F_0^2) + (aP)^2 + bP]$ where $P = (\max(F_0^2 \text{ or } 0) + 2F_c^2)/3$. [e] Two independent guanidinium and phosphate moieties in the unit cell.

H, amide-H*), 8.12 (d, 2 H, H4/4′, $^3J_{3,4}$ = 9 Hz), 8.01 (d, 2 H, H 5/5′, $^3J_{5,6}$ = 8 Hz), 7.87 (s, 2 H, isonicotinium-H3/5), 7.78 (s, 1 H, amide-H*), 7.52–7.47 (m, 4 H, H6/6′ and H3/3′), 7.34 (t, 2 H, H7/7′, $^3J_{6,7,8}$ = 8 Hz) and 7.22 (d, 2 H, H8/8′, $^3J_{7,8}$ = 8 Hz). ^{13}C NMR (d_6-DMSO): 165.7 (isonicotinium-*C*ONH$_2$), 148.7 (isonicotinium-C2/2′), 148.3 (C2/2′), 142.8 (isonicotinium-C4/4′), 132.2 (C8a/8a′), 130.8 (C4a/4a′), 130.6 (C4/C4′), 128.5 (C5/5′), 126.6 (isonicotinium-C3/3′), 126.0 (C7/7′, C8/8′), 125.1 (C6/6′), 121.6 (C3/3′) and 121.2 (C1/1′). $[\alpha]^{25} = 0°$ (measured at 2.2 mg cm^{-3} in CH$_3$OH).

* The following mesomeric resonance structure leads to an amide rotational barrier of +14.1 ± 0.2 kcal mol^{-1} around the C–N bond, which renders the two NH$_2$ protons inequivalent.[35]

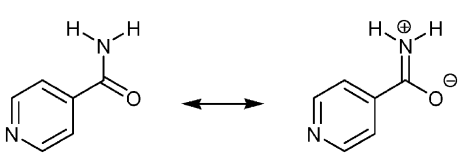

(Isonicotin-1-ium acid)-(*R*-1,1′-binaphthalene-2,2′-diyl phosphate), ($C_6H_6NO_2$)($C_{20}H_{12}PO_4$) (2). *R*-BNPPAH (0.174 g, 0.50 mmol), guanidinium chloride (0.048 g, 0.50 mmol) and isonicotinic acid (0.062 g, 0.50 mmol) were dissolved in a mixture of 10 cm^3 methanol and 5 cm^3 water. Evaporation of the solvent at room temperature yielded light-yellow crystals after 5–7 d (yield 0.17 g, 72%, average from four batches) (m.p. > 180 °C). $C_{26}H_{18}NO_6P$ (471.38): calc. C, 66.25; H, 3.85; N, 2.97; found C, 65.49; H, 4.06; N, 2.93%. IR (cm^{-1}): 1669 (s), 1590 (s), 1507 (s), 1465 (s), 1431 (m), 1328 (s), 1240 (s), 1100 (s), 992 (m), 962 (m), 855 (s), 746 (m) and 568 (m). ^{1}H NMR (d_6-DMSO): 8.79 (s, 2 H, isonicotinium-H2/6), 8.14 (d, 2 H, H4/4′, $^3J_{3,4}$ = 8 Hz), 8.01 (d, 2 H, H 5/5′, $^3J_{5,6}$ = 10 Hz), 7.88 (s, 2 H, isonicotinium-H3/5), 7.54 (d, 8 Hz, H3/3′, $^3J_{3,4}$ = 2 Hz), 7.50 (t, 2 H, H6/6′, $^3J_{5,6,7}$ = 6 Hz), 7.31 (t, 2 H, H7/7′, $^3J_{6,7,8}$ = 8 Hz) and 7.22 (d, 2 H, H8/8′, $^3J_{7,8}$ = 8Hz). ^{13}C NMR (d_6-DMSO): 165.7 (isonicotinium-*C*OOH), 149.5 (isonicotinium-C2/2′), 148.0 (C2/2′), 139.4 (isonicotinium-C4/4′), 131.8 (C8a/8a′), 130.9 (C4a/4a′), 130.7 (C4/C4′), 128.6 (C5/5′), 126.8 (isonicotinium-C3/3′), 126.0 (C7/7′ and C8/8′), 125.1 (C6/6′), 121.5 (C3/3′) and 121.0 (C1/1′). $[\alpha]^{25} = -452°$ cm^2 g^{-1} (measured at 2.5 mg cm^{-3} in CH$_3$OH; this corresponds to $[\alpha]^{25} = -611°$ cm^2 g^{-1} for a content of 73.7 wt% of BNPPA).

(Guanidinium)-(*rac*-1,1′-binaphthalene-2,2′-diyl phosphate)·dihydrate·semimethanol, (CH_6N_3)($C_{20}H_{12}PO_4$)·2H_2O·0.5-CH_3OH (3). *rac*-BNPPAH (0.174 g, 0.50 mmol) and

guanidinium carbonate (0.090 g, 0.50 mmol) were dissolved in a mixture of 10 cm^3 methanol and 10 cm^3 water. The solution was over-layered with 5 cm^3 of toluene. In the open vial, colorless, thin crystal plates formed after 3 days at room temperature at the methanol–water/toluene interface (yield 0.42 g, 92%, average from three batches) (m.p. > 180 °C). $C_{43}H_{48}N_6O_{13}P_2$ (doubled formula) (918.81): calc. C, 56.21; H, 5.27; N, 9.51; found C, 55.23; H, 5.46; N, 9.17%. IR (cm^{-1}): 1670 (s), 1590 (m), 1507 (m), 1464 (m), 1431 (m), 1328 (m), 1240 (m), 1099 (s), 991 (m) and 855 (m). ^{1}H NMR (d_6-DMSO): 8.05 (d, 2 H, H4/4′, $^3J_{3,4}$ = 9 Hz), 8.02 (d, 2 H, H5/5′, $^3J_{5,6}$ = 8 Hz), 7.44 (t, 2 H, H6/6′, $^3J_{5,6,7}$ = 5 Hz), 7.43 (d, 2 H, H3/3′, $^3J_{3,4}$ = 2 Hz), 7.30 (t, 2 H, H7/7′, $^3J_{6,7,8}$ = 8 Hz), 7.22 (d, 2 H, H8/8′, $^3J_{7,8}$ = 8 Hz), 7.14 (s, 6 H, guanidinium-H) and 3.20 (s, 1.5 H, methanol-CH_3). ^{13}C NMR (d_6-DMSO): 158.1 (guanidinium-C), 149.7 (C2/2′), 131.9 (C8a/8a′), 130.4 (C4a/4a′), 129.8 (C4/4′), 128.4 (C5/5′), 126.1 (C7/7′), 126.0 (C8/8′), 125.1 (C6/6′), 122.3 (C3/3′) and 121.6 (C1/1′).

***trans*-[Tetraammine-di(methanol ~ 0.75/aqua ~ 0.25)-copper(II)]-bis(*rac*-1,1′-binaphthalene-2,2′-diylphosphate) · dihydrate · monomethanol (4).** *rac*-BNPPAH (0.174 g, 0.50 mmol) and $Cu(NO_3)_2 \cdot 3H_2O$ (0.060 g, 0.25 mmol) were dissolved in a mixture of 10 cm^3 methanol and 5 cm^3 water, and 2 cm^3 of concentrated aqueous ammonia added. Evaporation at room temperature yielded blue thin crystal plates after a few days (yield 0.30 g, 61%, average from two batches) (m.p. > 180 °C). $C_{43.5}H_{54.5}CuN_4O_{14}P_2$ (982.89): calc. C, 53.16; H, 5.59; N, 5.70; found C, 53.15; H, 4.93; N, 5.65%. IR (cm^{-1}): 1617 (m), 1590 (m), 1464 (m), 1400 (m), 1329 (m), 1242 (s), 1102 (s), 992 (m), 963 (m), 850 (m), 749 (m), 657 (m) and 568 (m).

***trans*-(Diaqua-tetramethanol-copper(II))-bis(*rac*-1,1′-binaphthalene-2,2′-diylphosphate) · monohydrate · dimethanol (5).** *rac*-BNPPAH (0.070 g, 0.20 mmol), $Cu(NO_3)_2 \cdot 3H_2O$ (0.0241 g, 0.10 mmol) and isonicotinamide (0.0488 g, 0.40 mmol) were dissolved in a mixture of 10 cm^3 methanol and 5 cm^3 water. Evaporation at room temperature yielded greenish-blue thin plate-like crystals after a few days (yield 0.18 g, 90%, average from two batches) (m.p. > 180 °C) together with a bright blue solid (~10%). $C_{44}H_{46}CuO_{15}P_2 \cdot 2CH_3OH$ (1004.37): calc. C, 55.01; H, 5.41; $C_{44}H_{46}CuO_{15}P_2$ (940.33): calc. C, 56.20; H, 4.93; found C, 56.30; H, 4.93%. IR (cm^{-1}): 1591 (m), 1507 (m), 1464 (m), 1431 (m), 1328 (s), 1236 (s), 1098 (s), 992 (m), 945 (m), 870 (s), 818 (m), 748 (m), 720 (m), 697 (m), 567 (m) and 490 (m).

***cis*-[Diaqua-bis(ethylene diamine)-nickel(II)]-bis(*rac*-1,1′-binaphthalene-2,2′-diylphosphate) · dihydrate · dimethanol (6).** A solution of bis(ethylene diamine)nickel nitrate (0.09 g, 2.50 mmol) in 5 cm^3 of water was cooled to about 4 °C, over-layered with 5 cm^3 of methanol and a solution of *rac*-BNPPAH (0.174 g, 0.50 mmol) in 15 cm^3 of methanol. Pale violet thin crystal plates formed at the interface within a few hours (yield 0.21 g, 87%, average from three batches) (m.p. > 180 °C). $C_{46}H_{56}N_4NiO_{14}P_2$ (1009.60): calc. C, 54.72; H, 5.59; N, 5.55; found C, 54.10; H, 5.59; N, 5.26%. IR (cm^{-1}): 1589 (m), 1506 (m), 1463 (m), 1430 (w), 1368 (w), 1241 (m), 1241 (s), 1107 (s), 1070 (m), 991 (m), 962 (m), 943 (m), 868 (m), 850 (m), 816 (m), 748 (m), 718 (m), 697 (m), 657 (m), 580 (m), 566 (m) and 492 (m).

X-Ray crystallography

Data collection. Bruker AXS with CCD area detector, temperature 203(2) K for all structures, Enraf-Nonius Kappa CCD at 100(2) K for a second data set of **6**, Mo-K_α radiation (λ = 0.71073 Å), graphite monochromator, ω-scans, data collection and cell refinement using SMART,[36a] data reduction using SAINT,[36b] experimental absorption correction using SADABS, except for **5**.[37]

Structure analysis and refinement. The structures were solved by direct methods (SHELXS-97);[38a] refinement was done by full-matrix least-squares on F^2 using the SHELXL-97 program suite.[38b] All non-hydrogen positions were found and refined with anisotropic temperature factors.

Hydrogen atoms on the aromatic rings were placed at calculated positions with an appropriate riding model (AFIX 43) and an isotropic temperature factor of $U_{eq}(H) = 1.2U_{eq}(C)$. Hydrogen atoms on the methanol carbon atom were calculated as an idealized CH_3 group (AFIX 133) with $U_{eq}(H) = 1.5U_{eq}(C)$.

In **1**, **2** and **3**, the hydrogen atom(s) on the isonicotinium and guanidinium nitrogens, respectively, were found and refined with $U_{eq}(H) = 1.5U_{eq}(N)$. In **4**, the hydrogen atoms of the ammine ligands were calculated as idealized NH_3 groups with tetrahedral angles in a rotating group refinement (AFIX 137) and $U_{eq}(H) = 1.5U_{eq}(N)$. In **6**, the hydrogen atoms of the ethylene diamine ligands were calculated as idealized C/NH_2 groups with tetrahedral angles (AFIX 23) and $U_{eq}(H) = 1.2U_{eq}(C/N)$.

In **1**, **3** and **5**, the hydrogen atoms on oxygen (aqua ligands, water and methanol solvent of crystallization) were found and refined with $U_{eq}(H) = 1.5U_{eq}(O)$. In **2** and **6**, hydrogen atoms on oxygen (isonicotinium acid and water, respectively) were initially found but had to be kept fixed during further refinement with $U_{eq}(H) = 1.5U_{eq}(O)$. In **4**, one of the hydrogen atoms on the water of crystallization was found and refined with $U_{eq}(H) = 1.5U_{eq}(O)$. The other hydrogen of the water molecule was found but had to be fixed upon further refinement. In **4**, **5** and **6**, the methanol O–H groups (methanol ligands only in **5**) were placed at calculated positions as an idealized O–H group with a tetrahedral C–O–H angle and the formation of the best hydrogen bond to a neighboring acceptor (AFIX 83) made with $U_{eq}(H) = 1.5U_{eq}(O)$. Furthermore, in **4**, the methanol ligand was refined, together with a water ligand in the same position. This was done by keeping the oxygen atom as fully occupied and refining the occupancy of the methyl group to a value of ~0.75.

The structures of **6** at 203(2) K and 100(2) K were solved and refined in the non-centrosymmetric polar space group *Cc* with racemic twinning (twin law −1 0 0 0 −1 0 0 0 −1, BASF 0.478 95 at 203 K and 0.505 63 at 100 K). Structure solution and refinement was also carried out in the centrosymmetric space group *C*2/*c*. However, the $Ni(en)_2(H_2O)_2$ fragment was then found as crystallographically disordered due to the two-fold rotation axis in the vicinity of the nickel atom. The disorder could be fully resolved, yet refinement did not

Table 7 Crystal data and structure refinement for **6**

Compound	**6** at 203(2) K	**6** at 100(2) K
Empirical formula	$C_{46}H_{56}N_4NiO_{14}P_2$	$C_{46}H_{56}N_4NiO_{14}P_2$
M/g mol^{-1}	1009.60	1009.60
Crystal size/mm	0.41 × 0.40 × 0.04	0.36 × 0.34 × 0.04
θ range/°	0.97–25.60	3.26–26.70
h; k; l range	−51, 51; −11, 11; −15, 15	−53, 53; −10, 11; −15, 15
Crystal system	Monoclinic	Monoclinic
Space group	*Cc*	*Cc*
a/Å	42.599(8)	42.5440(18)
b/Å	9.0906(18)	9.0870(4)
c/Å	12.432(2)	12.3730(5)
α/°	90	90
β/°	98.762(4)	98.7550(19)
γ/°	90	90
V/Å^3	4758.1(16)	4727.6(3)
Z	4	4
D_{calc}/g cm^{-3}	1.409	1.418
F(000)	2120	2120
μ/mm^{-1}	0.545	0.549
Maximum/minimum transmission	0.9801/0.8053	0.9784/0.8269
Reflections collected	17756	15924
Independent reflections	8847 (R_{int} = 0.0653)	7505 (R_{int} = 0.0360)
Observed reflections [$I > 2\sigma(I)$]	5040	7043
Parameters refined	605	605
Maximum/minimum $\Delta\rho$ [a] /e Å^{-3}	2.278/−0.580	1.564/−0.770
R_1/wR_2 [$I > 2\sigma(I)$][b]	0.0514/0.0842	0.0431/0.1065
R_1/wR_2 (all reflections)[b]	0.1201/0.0982	0.0468/0.1092
Goodness-of-fit on F^2[c]	1.050	1.073
Weighting scheme w; a/b[d]	0.0000/7.9830	0.0575/9.9327

[a] Largest difference peak and hole. [b] $R_1 = [\Sigma(||F_o| - |F_c||)/\Sigma|F_o|]$; $wR_2 = [\Sigma[w(F_o^2 - F_c^2)^2]/\Sigma[w(F_o^2)^2]]^{\frac{1}{2}}$. [c] Goodness-of-fit = $[\Sigma [w(F_o^2 - F_c^2)^2]/(n - p)]^{\frac{1}{2}}$. [d] $w = 1/[\sigma^2(F_o^2) + (aP)^2 + bP]$ where $P = (\max(F_o^2 \text{ or } 0) + 2F_c^2)/3$.

progress below $R_1 = 0.1419$ for 3073 data with $I > 2\sigma(I)$, and $R_1 = 0.2105$ and $wR_2 = 0.3554$ for all 5786 data at 203 K. At 100 K the refinement in space group $C2/c$ did not progress below $R_1 = 0.1770$ for 6113 data with $I > 2\sigma(I)$, and $R_1 = 0.1832$ and $wR_2 = 0.4414$ for all 6666 data. An investigation of the refined *Cc* space group structures with PLATON and checkCIF did not suggest a space group change.

Details of the X-ray structure determinations and refinements are provided in Table 6 and Table 7.‡ Graphics were drawn with DIAMOND (version 3.0d).[39] Computations on the supramolecular interactions and rigid-body model libration corrections for the Cu–O bond distances (“Hirshfeld Rigid-Bond” test, mean square vibration amplitudes) in **5** were carried out using PLATON for Windows.[40]

Acknowledgements

We are greatly thankful to the University of Freiburg for financial assistance. We thank Dr. Manfred Keller for the collection of the crystallographic data set and the structure solution of **6** at 100 K.

References

1 See general textbooks of Biochemistry or Biology, *e.g.*, A. L. Lehninger, *Principles of Biochemistry*, Worth Publishers, New York, 1982, pp. 317.
2 P. Raghavaiah, S. Supriya and S. K. Das, *CrystEngComm*, 2005, **7**, 167.
3 (*a*) C. B. Aakeröy and A. M. Beatty, *Aust. J. Chem.*, 2001, **54**, 409; (*b*) B. Moulton and M. J. Zaworotko, *Chem. Rev.*, 2001, **101**, 1629; (*c*) G. R. Desiraju, *Chem. Rev.*, 1998, **98**, 1375; (*d*) G. R. Desiraju, *Crystal Engineering—The Design of Organic Solids*, Elsevier, Amsterdam, 1989.
4 Reviews: (*a*) L. Brammer, *Chem. Soc. Rev.*, 2004, **43**, 476; (*b*) G. R. Desiraju, *Acc. Chem. Res.*, 1999, **35**, 565; (*c*) D. Braga, F. Grepioni and M. J. Zaworotko, *Chem. Soc. Rev.*, 1994, **23**, 283; (*d*) S. Subramanian and M. J. Zaworotko, *Coord. Chem. Rev.*, 1994, **137**, 357; (*e*) M. J. Zaworotko, *Chem. Commun.*, 2001, 1.
5 C. Janiak, *J. Chem. Soc., Dalton Trans.*, 2000, 3885.
6 Recent π-interactions for comparison: (*a*) X.-J. Yang, F. Drepper, B. Wu, W.-H. Sun, W. Haehnel and C. Janiak, *Dalton Trans.*, 2005, 256 and supplementary material therein; (*b*) K. Abu-Shandi, H. Winkler, H. Paulsen, R. Glaum, B. Wu and C. Janiak, *Z. Anorg. Allg. Chem.*, 2005, **631**, 2705; (*c*) S. Banerjee, A. Ghosh, B. Wu, P.-G. Lassahn and C. Janiak, *Polyhedron*, 2005, **24**, 593; (*d*) S. Banerjee, B. Wu, P.-G. Lassahn, C. Janiak and A. Ghosh, *Inorg. Chim. Acta*, 2005, **358**, 535; (*e*) C. Zhang, G. Rheinwald, V. Lozan, B. Wu, P.-G. Lassahn, H. Lang and C. Janiak, *Z. Anorg. Allg. Chem.*, 2002, **628**, 1259; (*f*) E. Craven, E. Mutlu, D. Lundberg, S. Temizdemir, S. Dechert, H. Brombacher and C. Janiak, *Polyhedron*, 2002, **21**, 553; (*g*) C. Zhang and C. Janiak, *Z. Anorg. Allg. Chem.*, 2001, **627**, 1972; (*h*) C. Zhang and C. Janiak, *J. Chem. Crystallogr.*, 2001, **31**, 29; (*i*) C. Zhang, C. Janiak and H. Brombacher, *Z. Naturforsch., B: Chem. Sci.*, 2001, **56**, 1205; (*j*) M. Munakata, L. P. Wu and T. Kuroda-Sowa, *Adv. Inorg. Chem.*, 1999, **46**, 173.
7 (*a*) M. Nishio, *CrystEngComm*, 2004, **6**, 130; (*b*) M. Nishio, M. Hirota and Y. Umezawa, *The CH/π Interaction: Evidence, Nature and Consequences*, Wiley-VCH, New York, 1998; (*c*) Y. Umezawa, S. Tsuboyama, K. Honda, J. Uzawa and M. Nishio, *Bull. Chem. Soc. Jpn.*, 1998, **71**, 1207; (*d*) C. Janiak, S. Temizdemir, S. Dechert, W. Deck, F. Girgsdies, J. Heinze, M. J. Kolm, T. G. Scharmann and O. M. Zipffel, *Eur. J. Inorg. Chem.*, 2000, 1229.
8 (*a*) K. T. Holman, A. M. Pivovar, J.A. Swift and M. D. Ward, *Acc. Chem. Res.*, 2001, **34**, 107; (*b*) A. M. Pivovar, K. T. Holman and M. D. Ward, *Chem. Mater.*, 2001, **13**, 3018; (*c*) V. A. Russell, M. C. Etter and M. D. Ward, *J. Am. Chem. Soc.*, 1994, **116**, 1941.
9 (*a*) R. Imhof, E. Kyburz and J. J. Daly, *J. Med. Chem.*, 1984, **27**, 165; (*b*) S. H. Wilen, J. Z. Qi and P. G. Willard, *J. Org. Chem.*, 1991, **56**, 485; (*c*) N. Hirayama, T. Sugaya, S. Tomioka, E. Ohshima and H. Obase, *Acta Crystallogr., Sect. C: Cryst. Struct. Commun.*, 1993, **49**, 600; (*d*) R. Dorta, P. Egli, F. Zurcher and A. Togni, *J. Am. Chem. Soc.*, 1997, **119**, 10857; (*e*) J. M. Mathews, A. B. Dyatkin, M. Evangelisto, D. A. Gauthier, L. R. Hecker, W. J. Hoekstra, F. Liu, B. L. Poulter, K. L. Sorgi and B. E. Maryanoff, *Tetrahedron: Asymmetry*, 2004, **15**, 1259.
10 I. Fuji and N. Hirayama, *Helv. Chim. Acta*, 2002, **85**, 2946.
11 Recent examples: (*a*) A. Moghimi, S. Sheshmani, A. Shokrollahi, M. Shamsipur, G. Kickelbick and H. Aghabozorg, *Z. Anorg. Allg. Chem.*, 2005, **631**, 160; (*b*) M. Hemamalini, P. T. Muthiah, U. Rychlewska and A. Plutecka, *Acta Crystallogr., Sect. C: Cryst. Struct. Commun.*, 2005, **61**, o95; (*c*) M. Du and X.-J. Zhao, *Acta Crystallogr., Sect. E: Struct. Rep. Online*, 2004, **60**, o439; (*d*) T. Akutagawa, T. Hasegawa, T. Nakamura and G. Saito, *CrystEngComm*, 2003, **5**, 54; (*e*) S. Kawata, K. Adachi, Y. Sugiyama, M. K. Kabir and S. Kaizaki, *CrystEngComm*, 2002, **4**, 496.
12 T. Dorn, C. Janiak and K. Abu-Shandi, *CrystEngComm*, 2005, **7**, 633.
13 (*a*) B. Paul, C. Näther, K. M. Fromm and C. Janiak, *CrystEngComm*, 2005, **7**, 309; (*b*) B. Paul, C. Näther, B. Walfort, K. M. Fromm, B. Zimmermann, H. Lang and C. Janiak, *CrystEngComm*, 2004, **6**, 293.
14 D. A. Haynes, W. Jones and W. D. S. Motherwell, *CrystEngComm*, 2005, **7**, 342.
15 E. Craven, K. Abu-Shandi and C. Janiak, *Z. Anorg. Allg. Chem.*, 2003, **629**, 195.

16 For a similar analysis and sequence in hydrogen bonds to $Cl^{(-)}$ see: (*a*) G. R. Desiraju and T. Steiner, *The Weak Hydrogen Bond*, IUCr/Oxford University Press, London, 1999, ch. 3.2.1.2, pp. 215ff; (*b*) F. Zordan, S. L. Purver, H. Adams and L. Brammer, *CrystEngComm*, 2005, **7**, 350.
17 Examples with aqua and methanol ligands: (*a*) L. P. Battaglia, A. B. Corradi, L. Menabue, M. Saladini and M. Sola, *J. Chem. Soc., Dalton Trans*., 1987, 1333; (*b*) K. Abu-Shandi, C. Janiak and B. Kersting, *Acta Crystallogr., Sect. C: Cryst. Struct. Commun*., 2001, **57**, 1261; (*c*) Y. Rodriguez-Martin, J. Sanchiz, C. Ruiz-Perez, F. Lloret and M. Julve, *CrystEngComm*, 2002, **4**, 631; (*d*) E. Craven, C. Zhang, C. Janiak, G. Rheinwald and H. Lang, *Z. Anorg. Allg. Chem*., 2003, **629**, 2282.
18 *trans*-Diaqua-bis(methoxyacetato) with increasing temperature up to 325 K: (*a*) B. Jakob and D. Reinen, *Z. Naturforsch., B: Chem. Sci*., 1987, **42**, 1500; (*b*) K. Prout, A. Edwards, V. Mtetwa, J. Murray, J. F. Saunders and F. J. C. Rossotti, *Inorg. Chem*., 1997, **36**, 2820; (*c*) M. J. Bew, D. E. Billing, R. J. Dudley and B. J. Hathaway, *J. Chem. Soc. A*, 1970, 2640; (*d*) C. K. Prout, R. A. Armstrong, J. R. Carruthers, J. G. Forest, P. Murray-Rust and F. J. C. Rossotti, *J. Chem. Soc. A*, 1968, 2791.
19 $\{[Cu(2,3\text{-bis}\{2\text{-pyridyl}\}pyrazine)(H_2O)_2](BF_4)_2 \cdot 2H_2O\}_n$: H. Grove, J. Sletten, M. Julve, F. Lloret and L. Lezama, *Inorg. Chim. Acta*, 2000, **310**, 217.
20 $[Cu(2,6\text{-dipyrazol-1-ylpyridine})](BF_4)_2$: (*a*) N. K. Solanki, M. A. Leech, E. J. L. McInnes, F. E. Mabbs, J. A. K. Howard, C. L. Kilner, J. M. Rawson and M. A. Halcrow, *J. Chem. Soc., Dalton Trans*., 2002, 1295; (*b*) G. S. Beddard, M. A. Halcrow, M. A. Hitchman, M. P. de Miranda, C. J. Simmons and H. Stratemeier, *Dalton Trans*., 2003, 1028.
21 $[Cu(2,6\text{-bisoximomethylpyridine})](ClO_4)_2 \cdot 2(acetone)$ at 300 K: M. A. Halcrow, C. A. Kilner, J. Wolowska, E. J. L. McInnes and A. J. Bridgeman, *New J. Chem*., 2004, **28**, 228.
22 $[(HC(Ph_2PO)_3)_2Cu](ClO_4)_2 \cdot 2H_2O$ with increasing temperature up to 340 K: C. J. Simmons, H. Stratemeier, G. R. Hanson and M. A. Hitchman, *Inorg. Chem*., 2005, **44**, 2753.
23 $[Cu(H_2O)_6](BrO_3)_2$: A. C. Blackburn, J. C. Gallucci and R. E. Gerkin, *Acta Crystallogr., Sect. C: Cryst. Struct. Commun*., 1991, **47**, 2019.
24 $[Cu(pyrazole)_6]^{2+}$: T. Otieno, J. R. Blanton, M. J. Hatfield, S. L. Asher and S. Parkin, *Acta Crystallogr., Sect. C: Cryst. Struct. Commun*., 2002, **58**, m182.
25 Review: L. R. Falvello, *J. Chem. Soc., Dalton Trans*., 1997, 4463.
26 (*a*) D. E. Billing, *Inorg. Chim. Acta*, 1974, **11**, L31; (*b*) M. Kavana, D. R. Powell and J. N. Burstyn, *Inorg. Chim. Acta*, 2000, **297**, 351 and references therein.
27 (*a*) F. L. Hirshfeld, *Acta Crystallogr., Sect. A: Cryst. Phys., Diffr., Theor. Gen. Cryst*., 1976, **32**, 239; (*b*) R. E. Rosenfield Jr, K. N. Trueblood and J. D. Dunitz, *Acta Crystallogr., Sect. A: Cryst. Phys., Diffr., Theor. Gen. Cryst*., 1978, **34**, 828.
28 Achiral molecules in non-centrosymmetric space groups: E. Pidcock, *Chem. Commun*., 2005, 3457.
29 J. W. Steed and J. L. Atwood, *Supramolecular Chemistry*, Wiley, New York, 2000.
30 H.-J. Schneider and A. Yatsimirski, *Principles and Methods in Supramolecular Chemistry*, Wiley, New York, 2000.
31 (*a*) K. Ding, Y. Wang, L. Zhang, Y. Wu and T. Matsura, *Tetrahedron*, 1996, **52**, 1005; (*b*) E. Yashima, C. Yamamoto and Y. Okamoto, *J. Am. Chem. Soc*., 1996, **118**(17), 4036.
32 S. Miyano, M. Tobita and H. Hashimoto, *Bull. Chem. Soc. Jpn*., 1981, **54**, 3522.
33 Y. Y. Hoyano and R. E. Pincock, *Can. J. Chem*., 1980, **58**, 134.
34 C. A. Bunton, *Acc. Chem. Res*., 1970, **3**, 257.
35 G. M. Leskowitz, N. Ghaderi, R. A. Olsen, K. Pederson, M. E. Hatcher and L. J. Mueller, *J. Phys. Chem. A*, 2005, **109**, 1152.
36 (*a*) *SMART. Data collection program for the CCD area detector system*, Bruker Analytical X-Ray Systems, Madison, Wisconsin, USA, 1997; (*b*) *SAINT. Data reduction and frame integration program for the CCD area detector system*, Bruker Analytical X-Ray Systems, Madison, Wisconsin, USA, 1997.
37 G. M. Sheldrick, *SADABS, Program for area detector adsorption correction*, Institute for Inorganic Chemistry, University of Göttingen, Germany, 1996.
38 (*a*) G. M. Sheldrick, *SHELXS-97, Program for solution of crystal structures*, University of Göttingen, Germany, 1997; (*b*) G. M. Sheldrick, *SHELXL-97, Program for refinement of crystal structures*, University of Göttingen, Germany, 1997.
39 *DIAMOND version 3.0d for Windows*, Crystal Impact Gbr, Bonn, Germany, http://www.crystalimpact.com/diamond.
40 (*a*) A. L. Spek, *Acta Crystallogr., Sect. A: Found. Crystallogr*., 1990, **46**, C34; (*b*) A. L. Spek, *PLATON. A multi-purpose crystallographic tool*, Utrecht University, Utrecht, The Netherlands, 2005. Windows implementation, version 80205: L. J. Farrugia, University of Glasgow, Glasgow, UK, 2005.